MET O 11 TECHNICAL NOTE NO. 252

MOUNTAIN WAVE GENERATION BY MODELS OF FLOW OVER SYNOPTIC SCALE OROGRAPHY

M.J.P. Cullen and C.A. Parrett

Met O 11 (Forecasting Research)
Meteorological Office
London Road
Bracknell
Berkshire
England

March 1987

AM

MOUNTAIN WAVE GENERATION BY MODELS OF FLOW OVER SYNOPTIC SCALE OROGRAPHY

By M J P CULLEN and C A PARRETT

Meteorological Office, Bracknell

SUMMARY

Cross sections of a forecast of flow over the Alps using a high resolution limited area model are studied. They show considerable lee wave activity on the scale of the whole Alpine ridge, in addition to the expected lee cyclogenesis. These waves appear to have a larger horizontal scale than observed mountain waves, but similar vertical structure. They are examined further using a two dimensional model. The results suggest that the mechanism for suppression of wave activity by rotation may be deficient in the models and that better numerical procedures may be needed.

1. INTRODUCTION

Despite extensive recent work on the problem of synoptic scale flow over orography, there is still a large gap between the theoretical work, often using very simple linear models; and studies using modern forecast models. A companion paper attempts to extend the theoretical understanding towards nonlinear quantitative results. This paper examines forecast model performance more closely in order to check that it is realistic and to compare it with other recent studies, for instance Del'Osso and Radinovic (1984). Some disturbing features are found, in studying which the ALPEX or other similar data sets will be important. The paper concentrates on high resolution modelling of flow over well resolved mountain ranges and does not treat the question of the parametrization of sub grid-scale orography in numerical models.

Results from the Meteorological Office fine mesh model with grid lengths down to 37.5 km are examined to see whether the expected flow separation occurs. They show that large inertia-gravity waves are generated. The scale is larger in the horizontal than those observed by Hoinka (1984, 1985) and appear to be more related to the scale of the mountains than the model grid-length. Since the forcing by the cross mountain wind is also much less than in the case studied by Hoinka, the waves may be unphysical. The amplitude increases considerably as the grid length is reduced from 75 to 37.5 km and contaminates the forecast of the lee cyclone which had been quite successful in the 75 km integration. Del'Osso and Radinovic (1984) obtained a good forecast of a lee cyclone with a 50 km grid and a rather smoother representation of the orography. Detailed examination of their results shows a suggestion of a similar wave. Their case contained a weaker cross mountain flow than the one used in our paper, so their results do not necessarily conflict with ours.

To investigate this further, results are shown from a two dimensional version of the forecast model, using a cross section over the Alps taken from a three dimensional analysis and modified to be in exact thermal wind balance. The integration shows a large wave of the same horizontal scale as the mountain barrier. The results of Klemp and Lilly (1978) suggest that such a model correctly simulates the gravity wave response of flow over a ridge when the Coriolis term is unimportant. The close correspondence between their results and aircraft data suggest that the finite difference procedure is adequate for that type of flow. On larger scales the study of Williams and Hori (1970) shows that the tendency of the fluid to produce an unbalanced hydraulic jump reduces with Rossby number; and the work of Parrett and Cullen (1984) confirms the ability of finite difference models of the shallow water equations to reproduce this transition correctly. Results from applying the same finite difference procedure to a semi-geostrophic model are also shown, which suggest that it is hard for the scheme to compute a balanced solution. This numerical difficulty may contribute to excessive wave generation in primitive equation models. In three dimensions the tendency may be reinforced by a lack of the flow separatio described in reality by Buzzi and Tibaldi (1978) and illustrated by some of the ALPEX data.

2. RESULTS FROM A FORECAST MODEL

Three dimensional solutions for flow over the Alps are presented using a complete limited area forecasting model.

The model used is a limited area version of the Meteorological Office forecast model. The model is described in Gilchrist and White (1982). The finite difference formulation is described in Cullen (1983) and the physical parametrizations in Foreman (1983). Details of the boundary formulation and a fuller description of the model are given in Dickinson and Temperton (1984).

Results are shown using resolutions of $^3/_4^\circ$ latitude by $^{15}/_{16}^\circ$ longitude and of $^3/_8^\circ \times {}^{15}/_{32}^\circ$. The topography was extracted from a data set with 10' resolution to the coarser of the grids used. It is shown in Fig 1 (c). In order to illustrate the convergence of the finite difference solutions for a fixed mountain shape, the coarse resolution topography was then interpolated to the finer mesh. This was done to avoid numerical problems caused by grid-scale variations in the topography. Other experiments (not shown in this paper) extracted the topography on the fine mesh.

Initial data for this study were derived from a global analysis on a $1^1/_2^\circ \times 1^7/_8^\circ$ grid, interpolated as required. The topography was grown to its full height over the first three hours of the forecast. To provide the best illustration of the effect of the mountains on the flow, the forecasts shown are for data time 12Z on 2 March 1984. The 500 mb and PMSL charts for this time are shown in Fig 1(a) and (b) respectively. A deep depression over the North Sea and associated upper vortex transfer southeastwards during the subsequent 24 hours with a strong northerly flow becoming established over the Alps and a lee cyclone forming over the Gulf of Genoa.

Cross-sections along longitude 8.5°E, shown as the line AB in Fig 1 (c), are shown for the 18 hour forecasts. The forecast using the $^3/_4^\circ \times {}^{15}/_{16}^\circ$ grid i shown in Fig 2. Care is necessary in interpreting such cross sections, because the flow is not two dimensional. The frontal surface can clearly be seen in the potential temperature cross-section. There appears to be a wave downstream o the Alps with a half-wavelength of about 1° of latitude. The wave axis slopes northward with height and the vertical wave-length in the troposphere is very large. There is a large increase in amplitude at 250 mb in the lower stratosphere, directly above the top of the mountain. The northerly component of the wind is shown in Fig 2(b). There is a marked acceleration in a region above the mountain. There is no obvious sign of flow separation at the height of the ridge crest.

The vertical velocity (Fig 2(c)) shows the region of upslope ascent and a very strong downslope wind. These are associated with the standing wave in the potential temperature field. There is also a region of lee side

upward motion at all levels except the lowest. This is associated with the lee cyclone development as illustrated by Buzzi and Tibaldi (1978). In order to examine the amount of flow around rather than over the Alps a map of the wind at sigma level 0.87 is shown in Fig 3. The circulations associated with the original depression, now over Germany, and the lee cyclone are well seen. There is some ridging in the wind over the Alps, where the flow is attempting to balance the pressure field, but no sign of diversion of the wind round the barrier. Similar results were obtained from the levels above and below (0.79 and 0.935).

The same cross sections using a $^{3}/_{8}^{\circ} \times {}^{15}/_{32}^{\circ}$ grid in the forecast model are shown in Fig 4. The potential temperature cross section (Fig 4(a)) shows a sharper frontal surface with the wave better defined. The wavelength is now nearer 3°, though there are shorter waves superposed on it. The maximum at 250 mb has led to two model layers having the same potential temperature and convection being released. The northerly wind (Fig 4(b)) shows a similar but more intense pattern over the mountain. The vertical velocity shows the same main features but additional shorter waves are superposed on it. Values reach 224 mb/hr, double those using the coarser grid.

These integrations were repeated using data from 12 hours earlier, when the flow over the Alps was slack and the initial growth of the mountains would not generate waves. They were also repeated without moisture and with vertical diffusion in the stratosphere. Different cross-sections were examine The forecasts were also carried out using a different position for the lateral boundary of the model. All the forecasts showed waves qualitatively similar to those illustrated. The vertical structure is consistent with interpretation of the waves as mountain-forced gravity waves. They are not, however, two dimensional. The transient details, however, were affected by the lateral boundary and the starting time of the forecast. The vertical diffusion only reduced the wave amplitude at upper levels. The use of "envelope" orography (Wallace et al., 1983), in which the mean mountain height over a

grid square is increased by adding the standard deviation of the orographic height within the grid square, increased the amplitude of the waves and the height of the maximum in the stratosphere.

3. TWO DIMENSIONAL MODEL RESULTS

a. Description of experiment

The gravity wave response of the forecast model is now studied by using a two dimensional model. On the horizontal scale of the case study, the Coriolis term is important; the Rossby radius associated with the Alps is of order 200 km. Williams and Hori (1970) show that the effect of the Coriolis term is to make waves less likely. We study here to what extent waves are suppressed in an integration using a two-dimensional cross section of the previous experiment. The data were chosen as a typical section, and modified so as to be in exact thermal wind balance. Verification of the model against the true evolution is thus not appropriate, the interest is the amplitude of the wave response.

The finite difference scheme uses staggered variables and second order centred differencing. The difference equations are, in the standard notation

$$\delta_x u = \left(u(x + \tfrac{1}{2}\Delta x) - u(x - \tfrac{1}{2}\Delta x) \right) / \Delta x$$

$$\bar{u}^x = \tfrac{1}{2}\left(u(x - \tfrac{1}{2}\Delta x) + u(x + \tfrac{1}{2}\Delta x) \right) \quad :$$

$$\delta_t \bar{u}^t = -\tfrac{1}{2}\delta_{2x}(u^2) - \overline{\dot{\sigma}^x \delta_\sigma u}^\sigma + f\bar{v}^x - \delta_x \phi - R\bar{T}^x \delta_x \ln p_* + K_u p_*^{-1} \delta_x p_* \delta_x u ,$$

$$\delta_t \bar{v}^t = -\overline{u \delta_x v}^x - \overline{\dot{\sigma} \delta_\sigma v}^\sigma - f\bar{u}^x + K_v p_*^{-1} \delta_x p_* \delta_x v ,$$

$$\delta_t \bar{\theta}^t = -\overline{u \delta_x \theta}^x - \overline{\dot{\sigma} \delta_\sigma \theta}^\sigma + K_\theta p_*^{-1} \delta_x p_* \delta_x \theta ,$$

$$\delta_t \bar{p}_*^t + \delta_x (u \bar{p}_*^x) + \delta_\sigma (\dot{\sigma} \bar{p}_*^\sigma) = 0 ,$$

$$\dot{\sigma} = 0 \qquad \text{at} \qquad \sigma = 0, 1,$$

$$\delta_\sigma \phi = -\overline{RT\sigma^{-1}}^{\sigma} .$$

K_u, K_v and K_θ are artificial viscosity coefficients. The form of the viscosity is chosen to ensure mass and momentum conservation. If a hydraulic jump is formed in the solution it can then be treated correctly, Parrett and Cullen (1984). To prevent possible reflections from the lateral boundaries, the viscosity is increased linearly over the four gridlengths next to the boundaries.

The initial shape of the mountain was given by

$$\phi_* = \tfrac{1}{2}H\left(\cos\left((x - x_0)/l\right) + 1\right) \qquad -l\pi \le (x - x_0) \le l\pi$$

$$= 0 \qquad \text{elsewhere.}$$

The equations were then solved with u = 0 at the ends of the channel and the mountain translated at a speed of 15 ms^{-1}. A uniform grid with 101 points in the horizontal and 20 in the vertical was used, giving a gridlength of 13 km. A convective adjustment scheme was found necessary, despite the lack of forcing terms, to deal with overturning mountain waves. A vertical diffusion scheme with a coefficient dependent on the local Richardson number was used. The coefficient was chosen to prevent the Richardson number based on grid point values falling below $\frac{1}{4}$ and was based on standard mixing length concepts.

b. Results of integrations

The initial fields used for the integrations, shown in Fig 5, were obtained from a typical cross-section of a three dimensional analysis across the Alps. This was done by extracting the wind component parallel to the mountain onto a grid, and calculating a geostrophically and hydrostatically balanced potential temperature field, ignoring the mountain. A smooth "sine-shaped" mountain was then introduced and θ interpolated onto sigma levels using a cubic spline, and from this a balanced v field was re-calculated. This process was preferred to the more usual method of growing orography at the start of a forecast, to try to eliminate excitation of spurious waves.

Figures 6 to 9 show the finite difference results after 12 hours of integration. The most striking feature of these is the large "jump-like" wave seen in the troposphere above and to the lee of the mountain; the isentropes (Fig 6) in the middle and lower troposphere have the same shape as the free surface in a hydraulic jump (eg Parrett and Cullen, 1984). This feature closely resembles the observations and numerical simulation of a strong mountain wave over the Rockies shown in Klemp and Lilly (1978), including the strong downslope wind (Figs 8 and 9) associated with the downward displacement of the isentropes above the lee slope, and the abrupt transition to strong upward motion downstream of the mountain peak associated with the jump in the isentropes.

The wave/jump feature is evident throughout the depth of the troposphere and slopes upstream with height indicating downward transfer of horizontal momentum, as expected in hydrostatic mountain waves and as seen in the computations and observations of Klemp and Lilly. The upstream tilt with height is more obvious at 6 hours (not shown), before the region downstream of the mountain becomes destabilised by the strong descent of high potential temperature air and its subsequent undercutting of lower potential temperature air. Similar areas of less stable air have been observed in the atmosphere, downstream of mountain ranges (Hoinka, 1984).

In Klemp and Lilly's observations there is a low-level wave and rotor downstream of the mountain range and here in our model there is something resembling a large rotor in the lee of the mountain associated with ascent (Fig 9) approximately one mountain width downstream of the peak. This ascending air seems to be partially returned towards the mountain near the top of the destabilised region at about 250 m and fed into the ascending part of the hydraulic jump. This return circulation is not seen in Klemp and Lilly's observations. Here, it seems to form part of a vertical wave in the cross-mountain flow (Fig 8), which is also seen above the mountain at a higher elevation.

Very large wind shears above the lee slope were obtained despite the inclusion of both horizontal and vertical diffusion to simulate turbulent mixing in regions where R_i is small. It was found that despite relatively large vertical diffusion coefficients being used in areas where $R_i \lesssim \frac{1}{4}$ it was impossible to keep $R_i > \frac{1}{4}$ in some areas above the lee slope. The vertical diffusion did have the effect of greatly reducing the otherwise very strong ($>$ 60 cm s^{-1}) upward motion approximately one mountain width downstream of the mountain.

Figure 10 shows the potential temperature field produced from a run that included a layer of enhanced vertical diffusion at the top of the model, which increased linearly upwards from just above the tropopause. One can see that part of the double-structured wave in the stratosphere evident in Fig 6 has been lost, indicating that this part of the wave, produced by reflection of wave energy from the upper boundary (and which slopes downstream with height), has been dissipated by the enhanced vertical diffusion. Other runs with increased horizontal diffusion towards the upper boundary (not shown), produced slightly less damping of the reflected wave, also tending to diffuse the wave directly and spread it out horizontally. This shows that it may be necessary to include a layer of high diffusion near the upper boundaries of numerical models to reduce such spurious reflected waves.

c. Two dimensional semi-geostrophic model

Both the primitive equation integrations described so far produce considerable wave activity. If this is not realistic, then either the numerical procedure is tending to excite waves, or the mechanism which tends to suppress them in the presence of rotation is not operating effectively. To provide further evidence, the two dimensional semi-geostrophic equations are integrated using the same finite difference procedure as for the primitive equations. These have to be solved implicitly for u and w. A procedure for doing so is described by Cullen and Purser (1984). The implicit equations are solved by a pseudo-time iteration which allows 10 times the physical time for the geostrophic adjustment process to operate.

The results can be compared qualitatively with the exact but low resolution Lagrangian solution described in the companion paper. The iteration does does not achieve convergence over the mountain top and there is a discrepency of 2.5 ms^{-1} in the geostrophic balance at high levels. The implied cross mountain wind is shown in Fig. 8(b). A region of upstream deceleration and the acceleration over the mountain top are predicted. However, the accelerations extend high up over the mountain with short wavelength oscillations in the vertical. This reflects the slow convergence of the iteration at high vertical wave numbers. A better procedure is clearly needed.

The difficulties in obtaining this solution, which should contain no waves, suggest that the finite difference procedure has great difficulty in maintaining a balanced solution. It is therefore not surprising that it readily generates waves when applied to the primitive equations.

4. DISCUSSION

The structure of the waves produced in the two dimensional integrations is very similar to that observed and predicted for flow over the Rockies by Klemp and Lilly (1978). Similar waves over the Alps and Pyrenees have been reported by Hoinka (1984, 1985). Rather similar waves appeared

in the three dimensional integrations. In all these cases the wavelength of the "hydraulic jump" was less than 1° of latitude. The vertical displacement of θ surfaces reached 2 km. The waves produced in our integrations have a large horizontal wavelength, apparently associated with the scale of the whole Alpine range. Their vertical amplitude and locations of regions of maximum intensity appear realistic.

There are several possible contributing mechanisms which may produce these waves. In the two-dimensional model all the flow is forced to cross the barrier. The finite difference scheme cannot follow the semi-geostrophic solution correctly in this case and produces large implied accelerations over the full depth of the fluid. When the same scheme is used in a primitive equation model this could lead to an excessive wave response. The Lagrangian semi-geostrophic solution suggests that large accelerations are only generated in small regions near the mountains, leading to a different type of wave response with localised generation. For the data used with mean flow speed around $15 ms^{-1}$, static stability $10^{-5} m^{-1}$ and density scale height 8 km, all waves with a wavelength of greater than the order of 10 km will propagate energy upwards and have an upstream phase slope. Thus there is a possibility that the lower stratospheric maximum and large general amplitude in the integrations are produced by wave trapping due to an unrealistic upper boundary condition. The experiments with vertical diffusion in the stratosphere are designed to allow absorption of the waves as they propagate up. Though these eliminate the reflected part of the wave, the overall reduction in amplitude is not dramatic, because most of the response is non-propagating.

Another contributor seems to be the failure of the flow to separate round the Alps, thus forcing much larger vertical velocities to be generated. ALPEX data, eg McGinley (1984), suggests a much greater degree of separation than is evident from Fig 3. This would suggest a failure of the integration

scheme to produce the correct three dimensional flow. If this explanation is correct, much further work will be needed to establish on what scales the correct physical solution is not obtained and what integration techniques are needed to get the correct solution in all cases, allowing for the dependence on scale and static stability. The results from the ECMWF model (Del'Osso and Radinovic (1984)) show a weak wave (their Fig 7). At some other times in their integrations (private communication) a stronger wave is visible. The difference in the synoptic situation at verification time in their case makes it difficult to assess whether there is sufficient flow separation. Considerable further work, taking advantage of ALPEX and similar data sets, will be required to resolve this issue.

ACKNOWLEDGEMENTS

The authors wish to thank Dr M W Moncrieff (Imperial College) for advice on gravity wave propagation, L Dell'Osso (ECMWF) for providing additional diagnostics from the ECMWF integrations, and Dr G J Shutts (Meteorological Office) and Dr. S Tibaldi (ECMWF) for helpful advice.

REFERENCES

Buzzi, A and Tibaldi, S 1978 Cyclogenesis in the lee of the Alps: a case study. Quart. J. Roy. Meteor. Soc., 104, 271-287.

Cullen, M J P 1983 Current progress and prospects in numerical techniques for weather prediction models. J.Comp.Phys., 50, 1-37.

Cullen, M J P and Purser, R J 1984 An extended Lagrangian theory of semi-geostrophic frontogenesis. J.Atmos. Sci., 41, 1477-1497.

Del'Osso, L and Radinovic, D 1984 A case study of cyclone development in the lee of the Alps on 18 March 1982. Beitr. Phys. Atmos., 57, 369-379.

Dickinson, A and Temperaton, C 1983 The operational numerical weather prediction model. UK Met.Office, Met O 11 Tech. Note no. 183.

Foreman, S J 1983 The numerical weather prediction model of the Meteorological Office. Amer.Meteor. Soc., 6th Conf. on Num.Weather Prediction, Omaha, Nebraska, 96-101.

Gilchrist, A and White, P W 1982 The development of the Meteorological Office new operational forecasting system. Meteor. mag., 111, 161-179.

Hoinka, K P 1984 Observations of a mountain wave event over the Pyrenees. Tellus, 36A, 369-383.

1985 Observations of the airflow over the Alps during a Foehn event. Quart. J.Roy. Meteor. Soc., 111, 199-224.

Klemp, J B and Lilly, D K 1978 Numerical simulation of hydrostatic mountain waves. J. Atmos. Sci., 35, 78-107.

McGinley, J A 1984 Scaling and theoretical considerations in variational analysis of flow around mountains. Beitr. Phys. Atmos., 57, 527-535.

Parrett, C A and Cullen, M J P 1984 Simulation of hydraulic jumps in the presence of rotation and mountains. Quart. J. Roy. Meteor. Soc., 110, 147-165.

Wallace, J M, Tibaldi, S and Simmons, A J 1983 Reduction of systematic forecast errors in the ECMWF model through the introduction of an envelope orography. Quart. J. Roy. Meteor. Soc., 109, 683-717.

Williams, R T and Hori, A M 1970 Formation of hydraulic jumps in a rotating system. J. Geophys. Res., 75, 2813-2821.

List of figures

Figure 1 Initial data for limited area model forecasts valid 12 GMT, 2 March 1984:

(a) 500 mb height (m), contour interval 30 m;

(b) PMSL (mb), contour interval 2 mb;

(c) topographic height (m), contour interval 200 m.

Figure 2 Cross section along line AB in Fig 1 (c) using $\frac{3}{4}^{\circ} \times \frac{15}{16}^{\circ}$ grid, valid 06 GMT, 3 March 1984;

(a) potential temperature (°C);

(b) wind normal to mountain (ms^{-1});

(c) vertical velocity (mb/hr).

Figure 3 Wind forecast at sigma = 0.87, forecast as Fig 2. Full feather 10 knots.

Figure 4 As Fig 2, using $\frac{3}{8}^{\circ} \times \frac{15}{32}^{\circ}$ grid:

(a) potential temperature (°C);

(b) wind normal to mountain (ms^{-1});

(c) vertical velocity (mb/hr);

Figure 5 Initial data for two dimensional integrations: (a) potential temperature (K), (b) wind parallel to mountain (ms^{-1}).

Figure 6 12 hour two dimensional primitive equation forecast: potential temperature (K).

Figure 7 As Fig 6: wind parallel to mountain (ms^{-1}).

Figure 8 Wind normal to mountain at 12 hours (ms^{-1}): (a) primitive equation, (b) semi-geostrophic.

Figure 9 As Fig 6: vertical velocity (cm s^{-1}).

Figure 10 As fig 6: including vertical diffusion in the stratosphere.

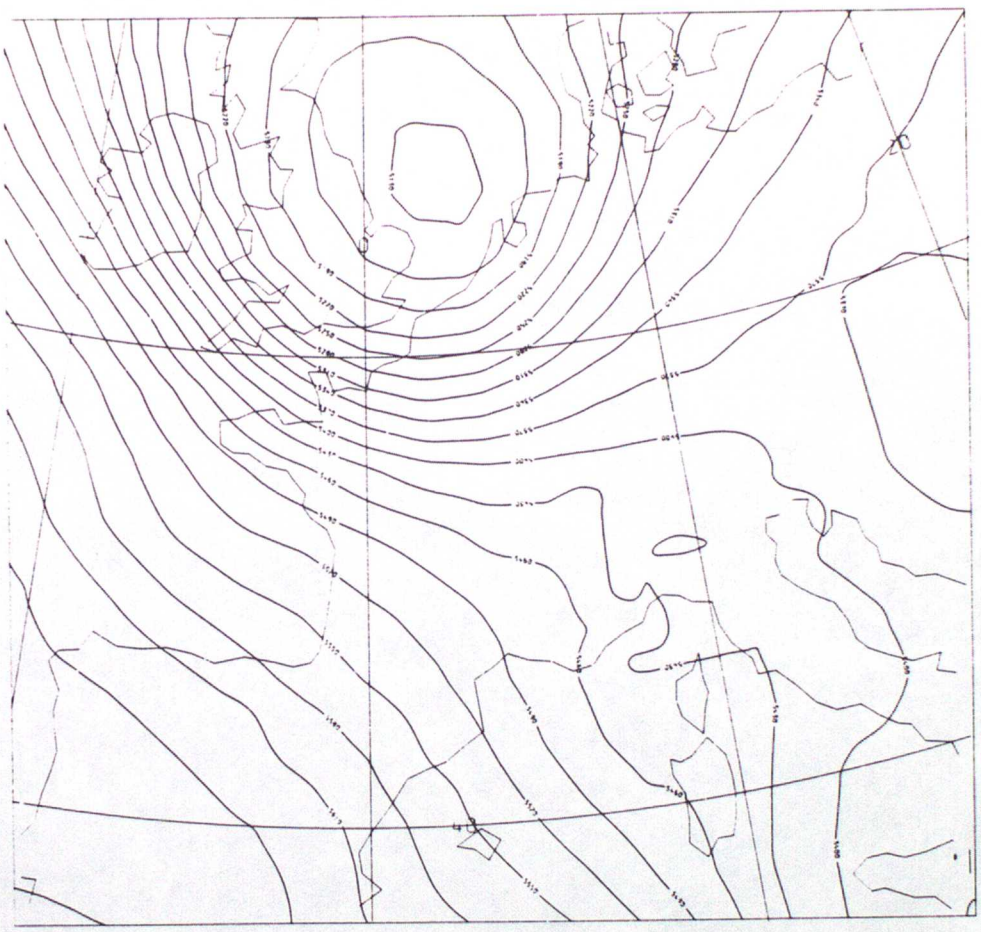

FIG. 1 (a)

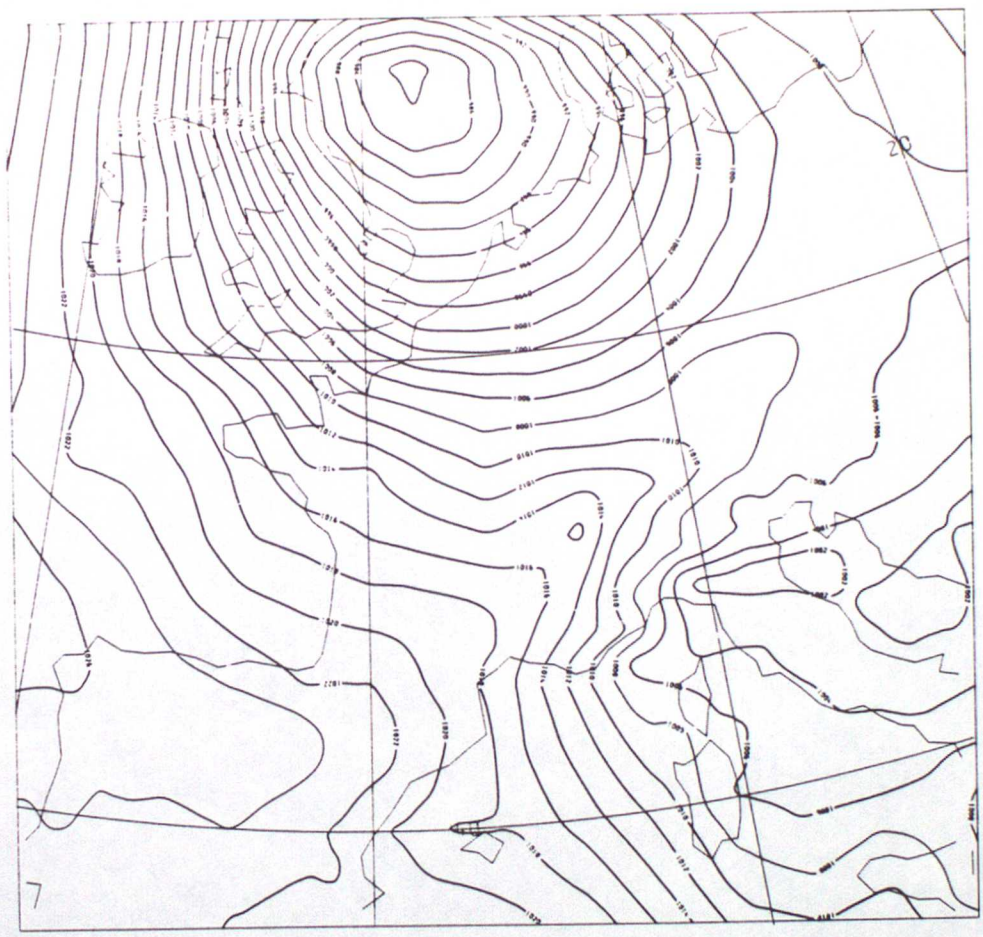

FIG. 1 (b)

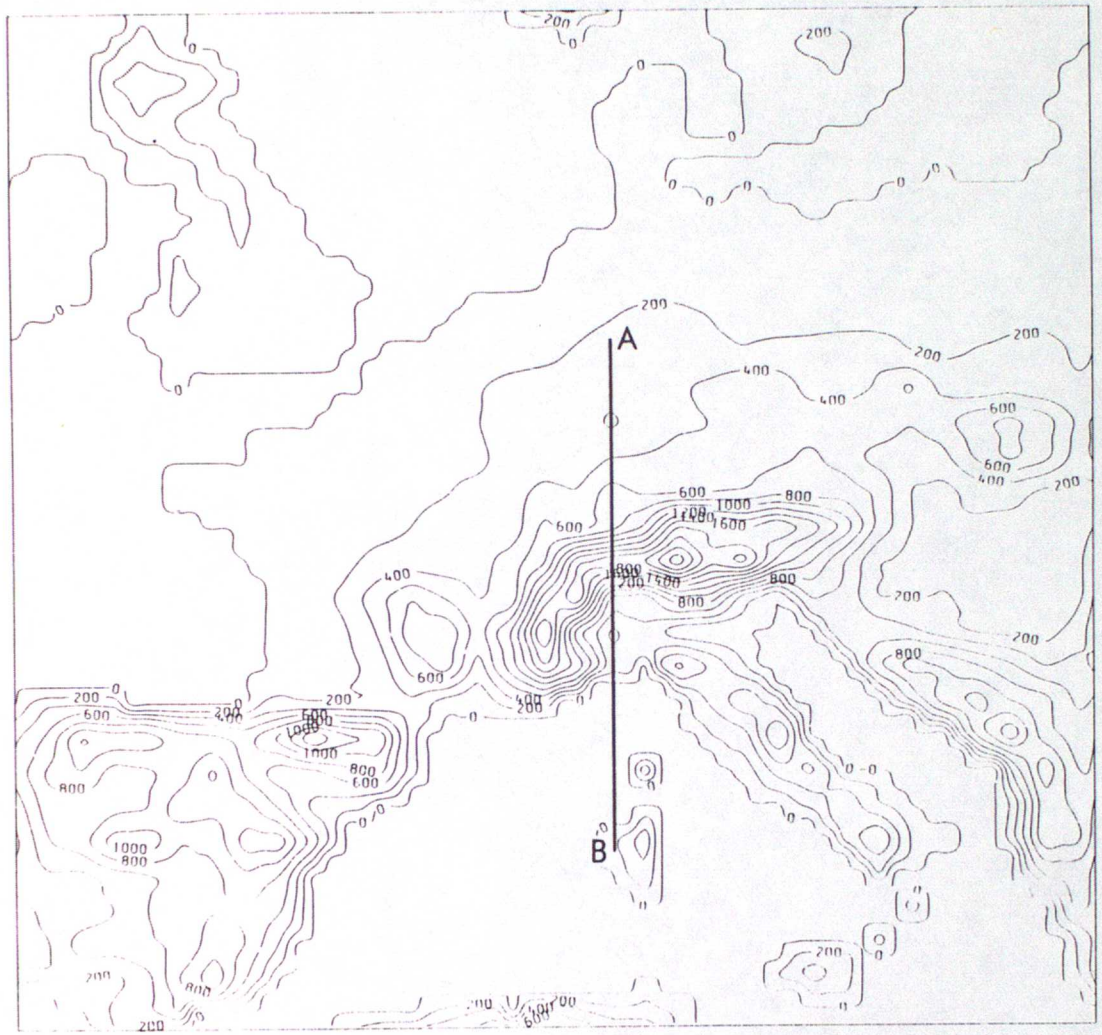

Fig. 1(c)

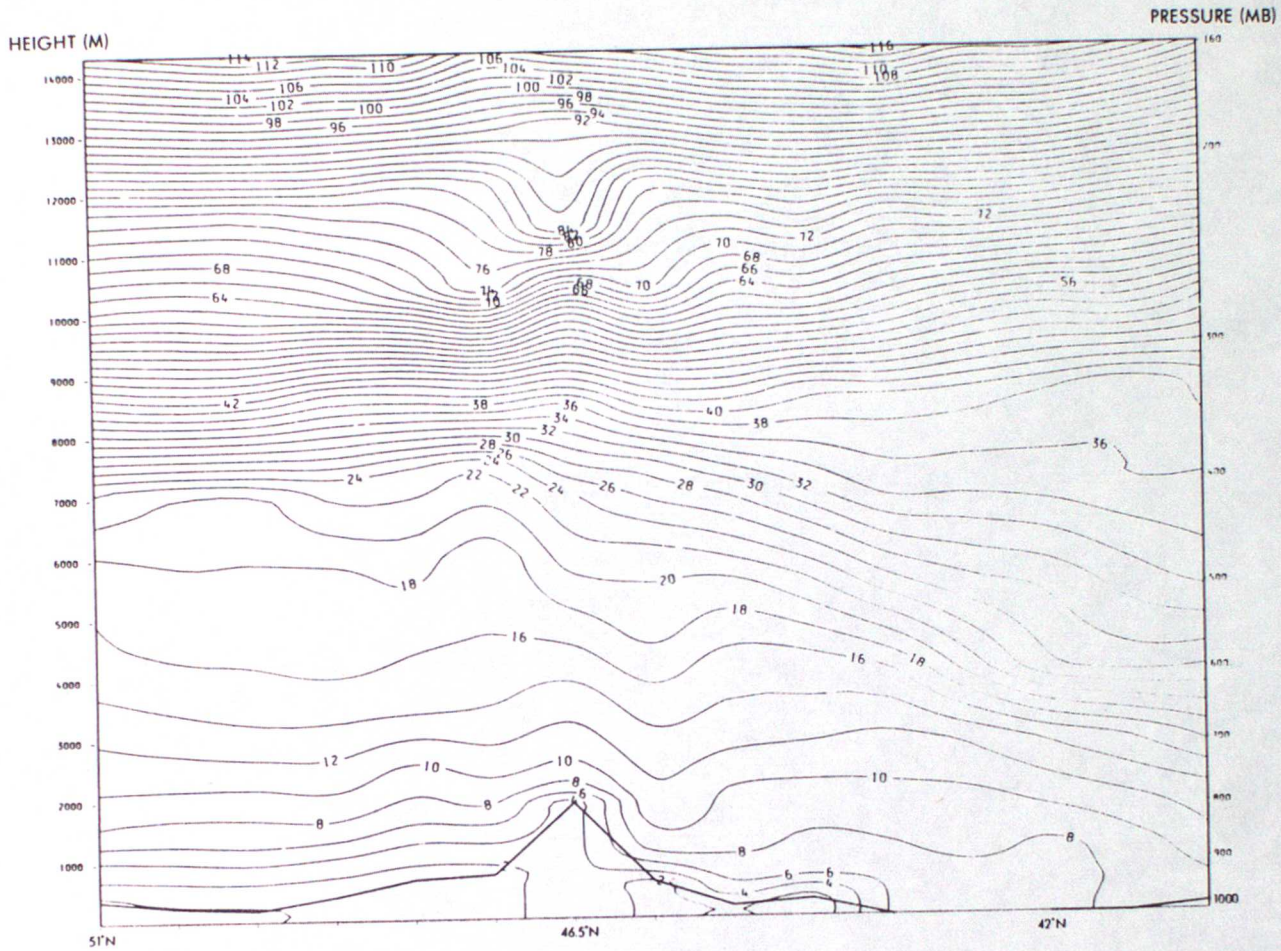

Fig 2 (a)

Fig 2 (b)

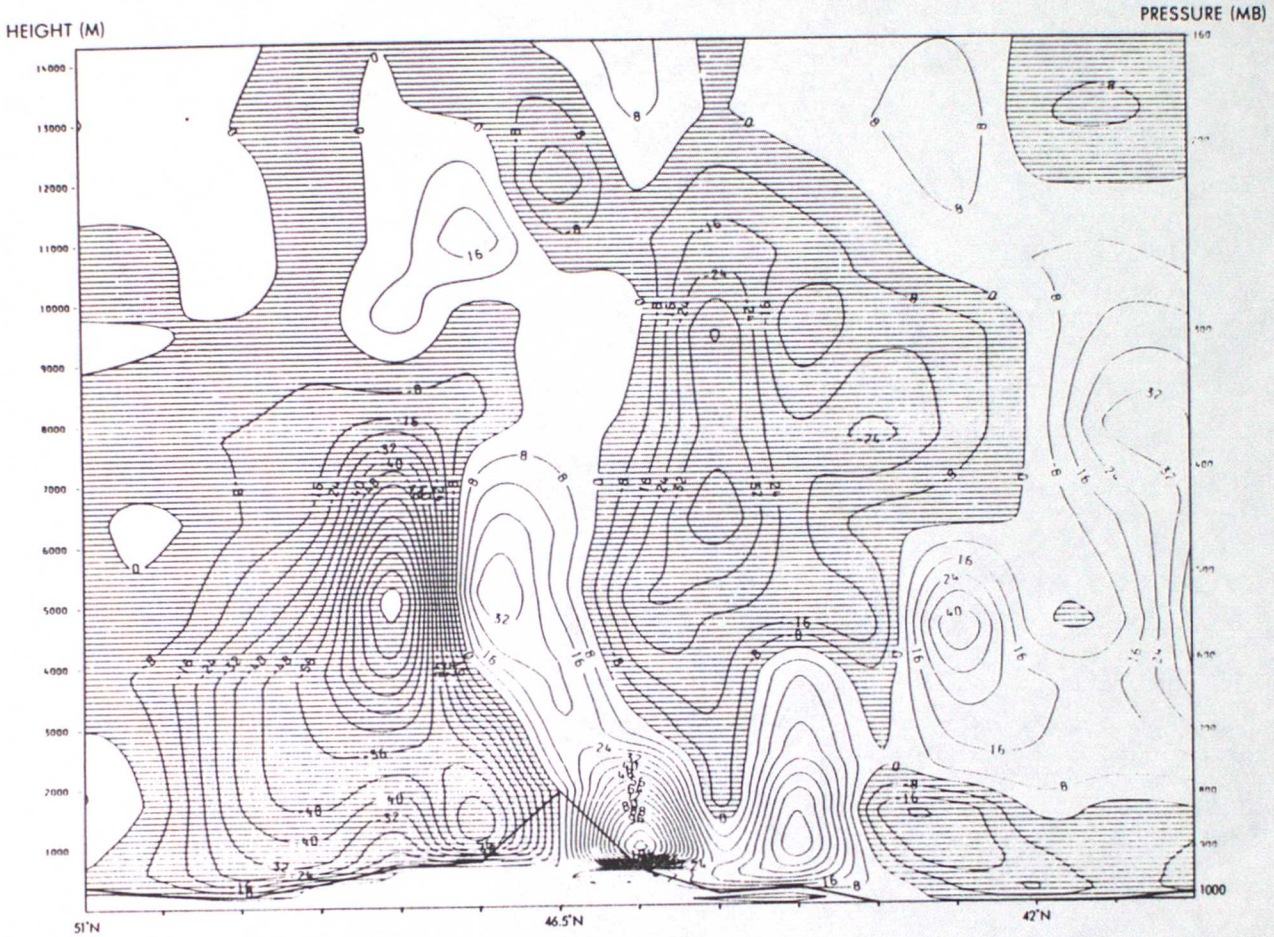
HEIGHT (M)
PRESSURE (MB)
14000
13000
12000
11000
10000
9000
8000
7000
6000
5000
4000
3000
2000
1000
1000
51°N
46.5°N
42°N

Fig 2 (c)

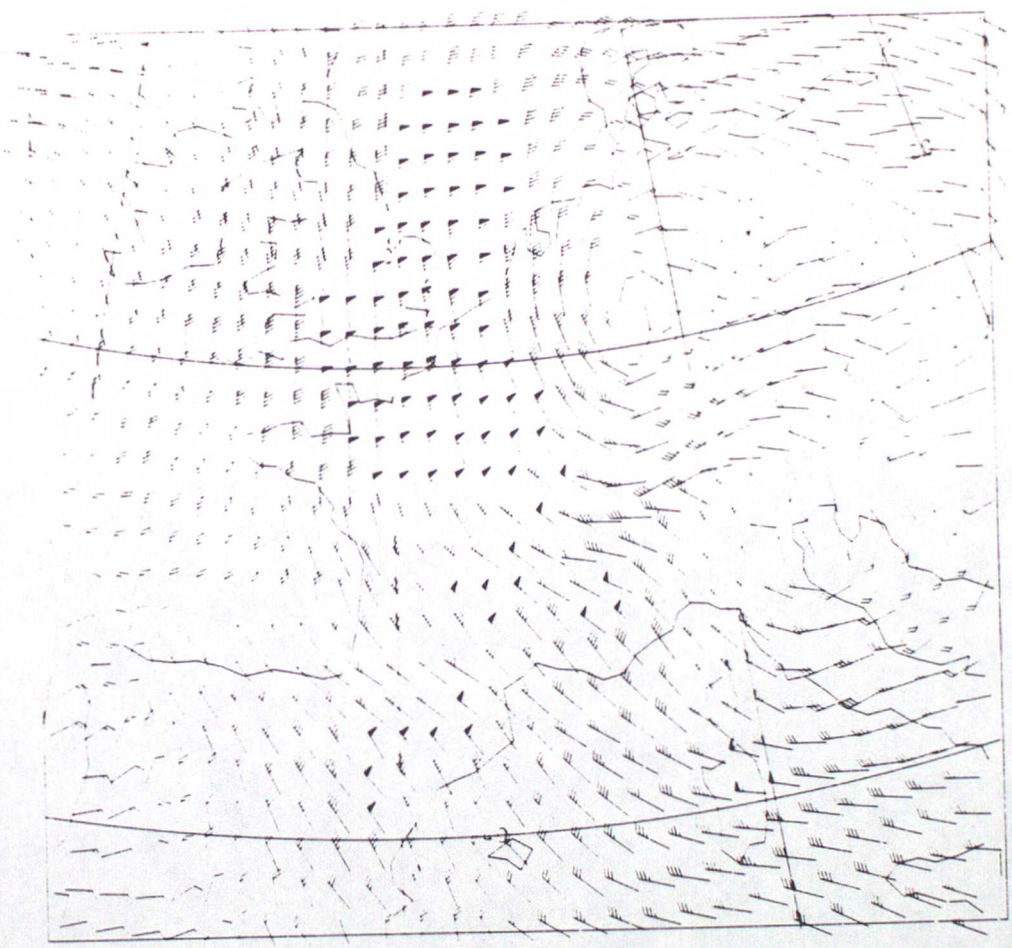

FIG. 3

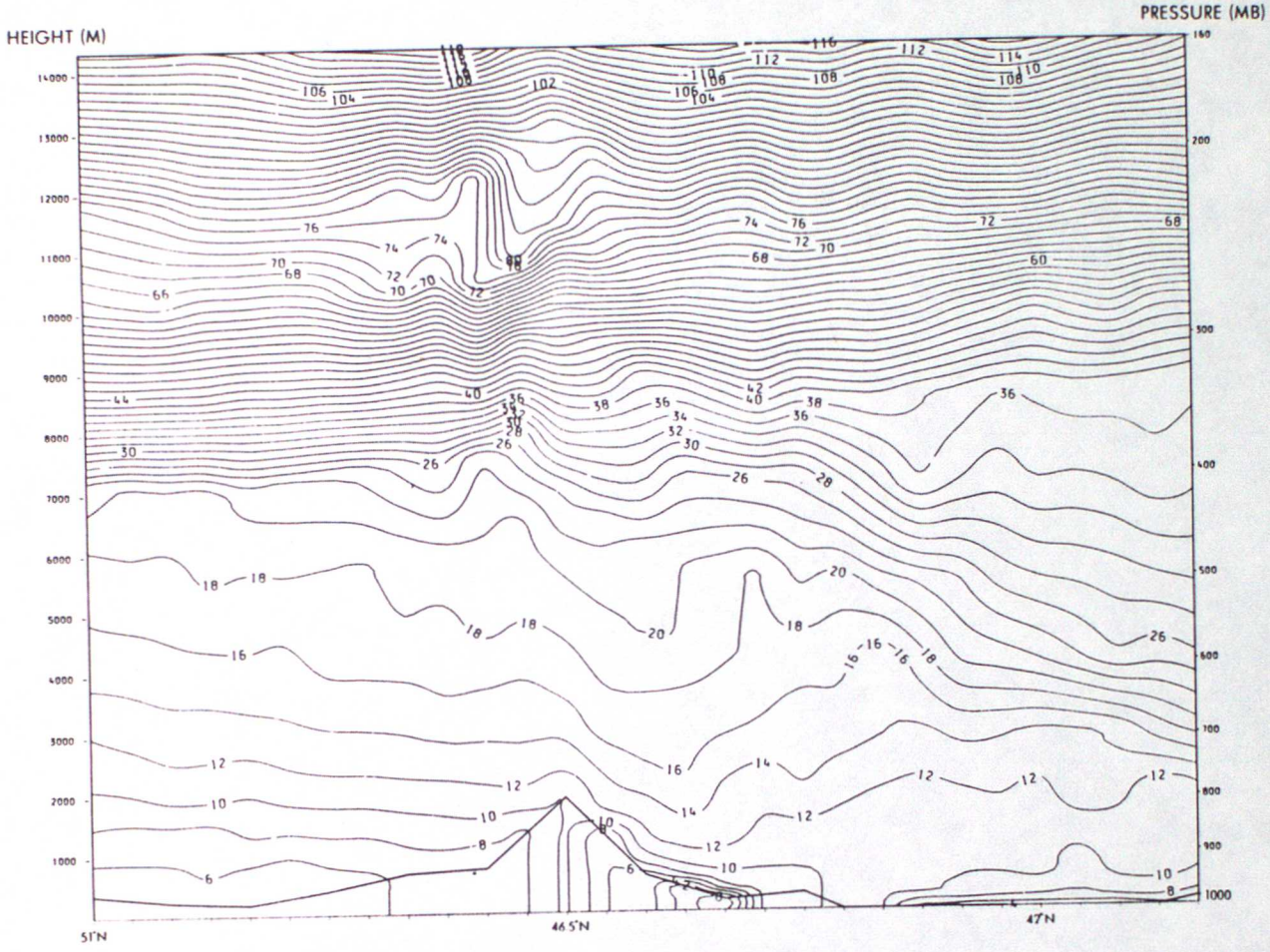
HEIGHT (M)
PRESSURE (MB)
14000
13000
12000
11000
10000
9000
8000
7000
6000
5000
4000
3000
2000
1000
150
200
300
400
500
600
700
800
900
1000
51°N
46.5°N
42°N

Fig. 4 (a)

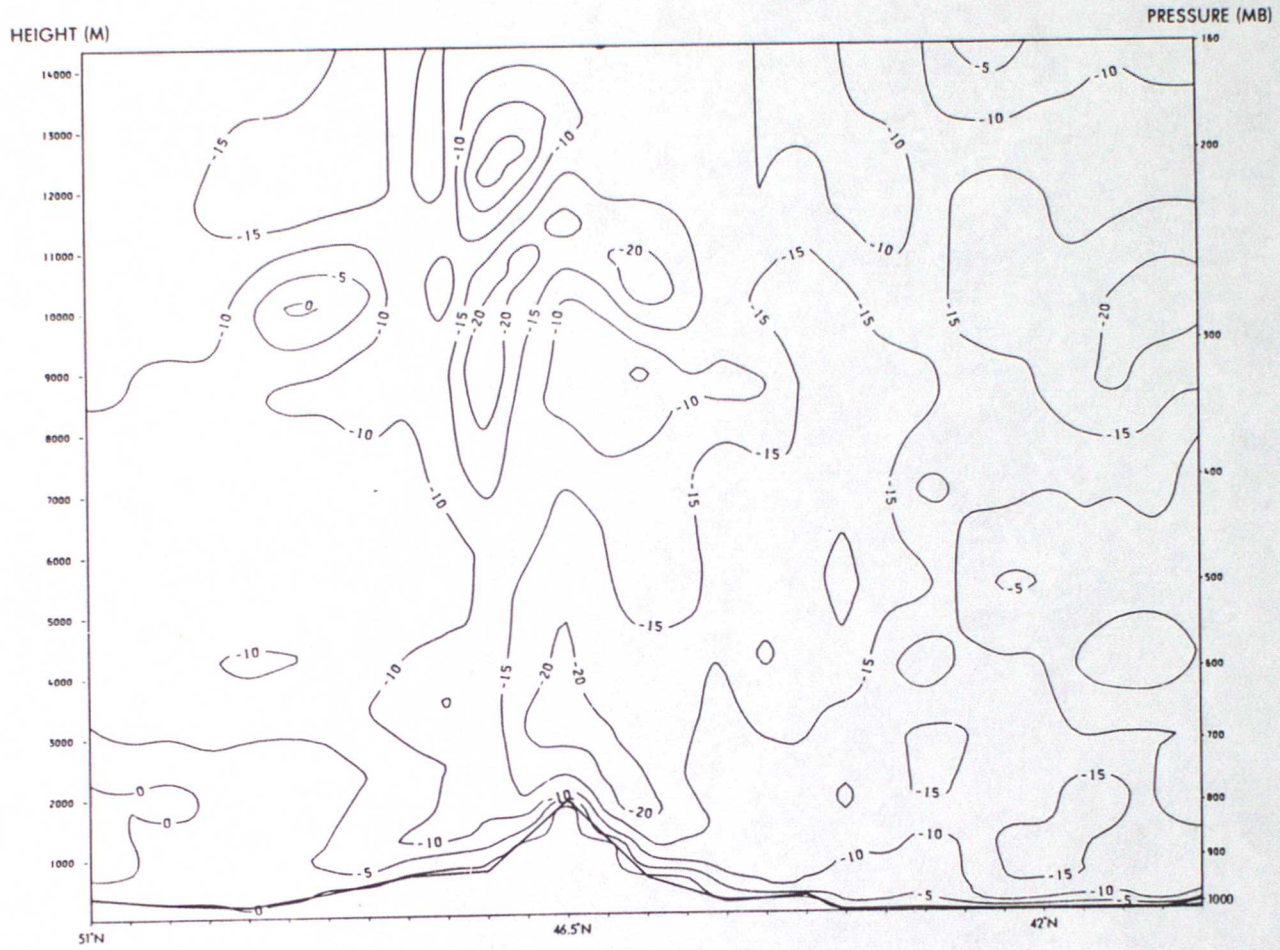
HEIGHT (M)
PRESSURE (MB)
14000
15000
12000
11000
10000
9000
8000
7000
6000
5000
4000
3000
2000
1000
160
200
300
400
500
600
700
800
900
1000
51°N
46.5°N
42°N

Fig. 4(b)

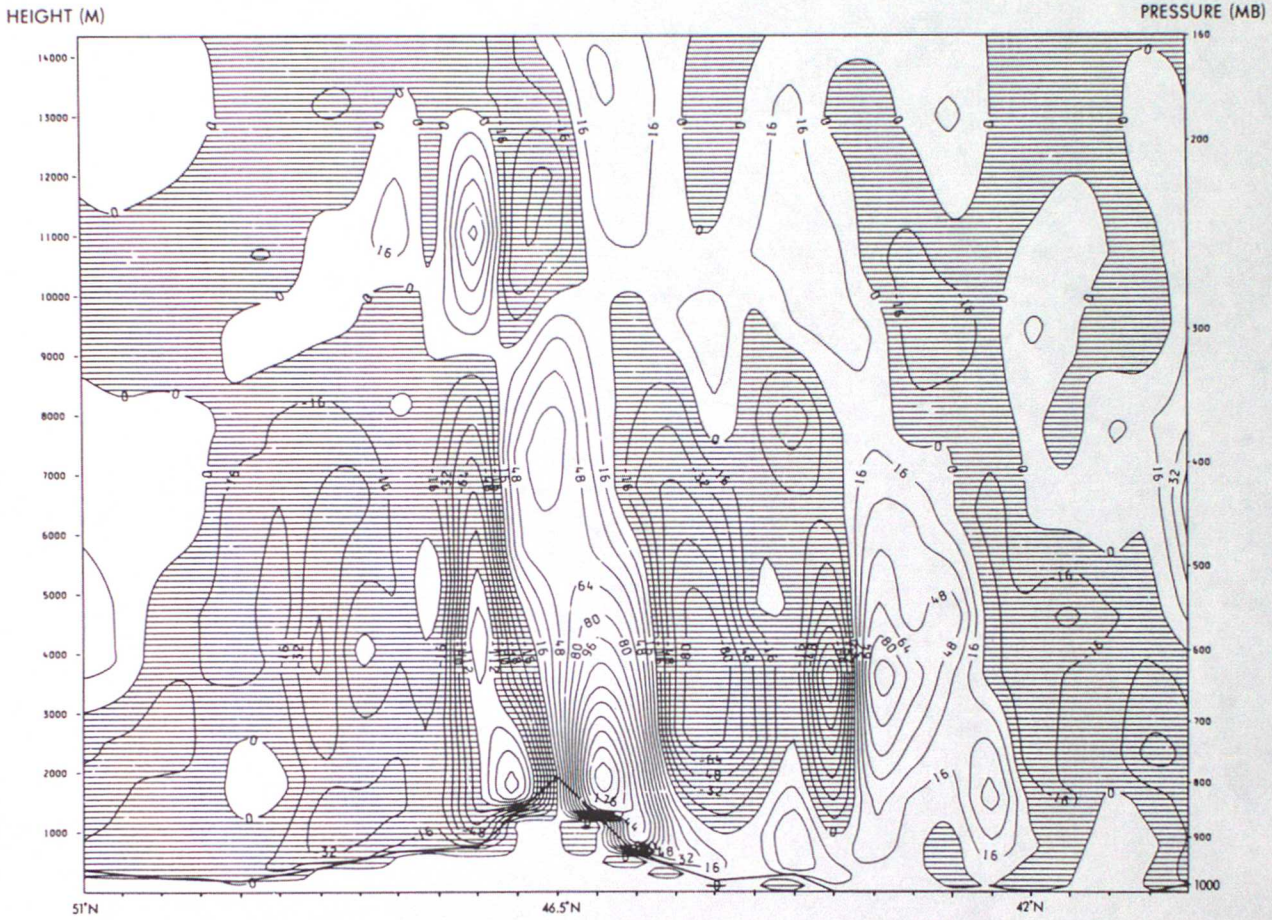
HEIGHT (M)
PRESSURE (MB)
14000
13000
12000
11000
10000
9000
8000
7000
6000
5000
4000
3000
2000
1000
160
200
300
400
500
600
700
800
900
1000
51°N
46.5°N
42°N

Fig. 4(c)

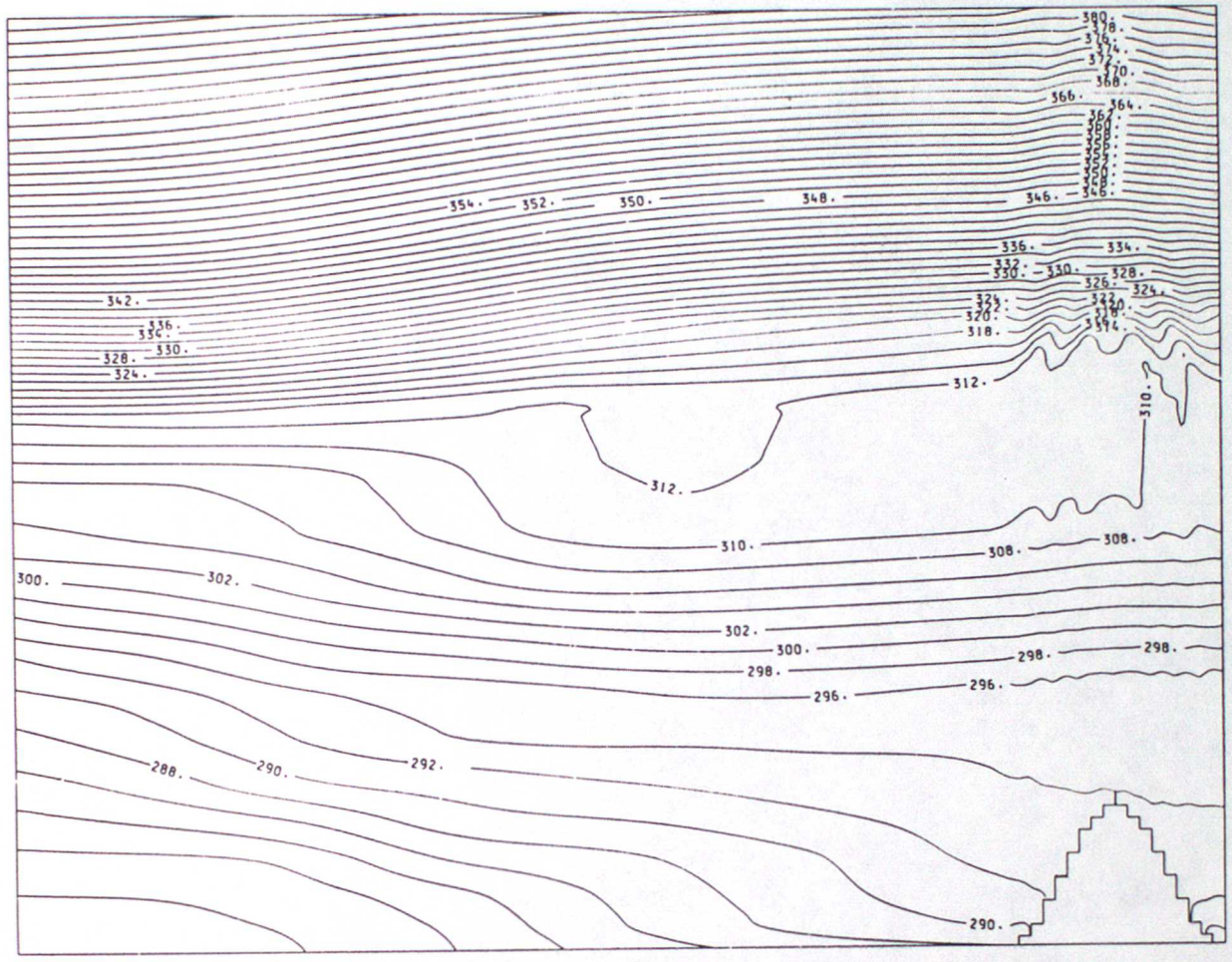
380.
378.
376.
374.
372.
370.
368.
366.
364.
354.
352.
350.
348.
346.
336.
334.
332.
330.
328.
326.
324.
322.
320.
318.
316.
314.
342.
340.
338.
336.
334.
332.
330.
328.
326.
324.
312.
312.
310.
310.
308.
308.
300.
302.
302.
300.
298.
298.
298.
296.
296.
292.
290.
288.
290.

Fig. 5(a)

Fig. 5 (b)

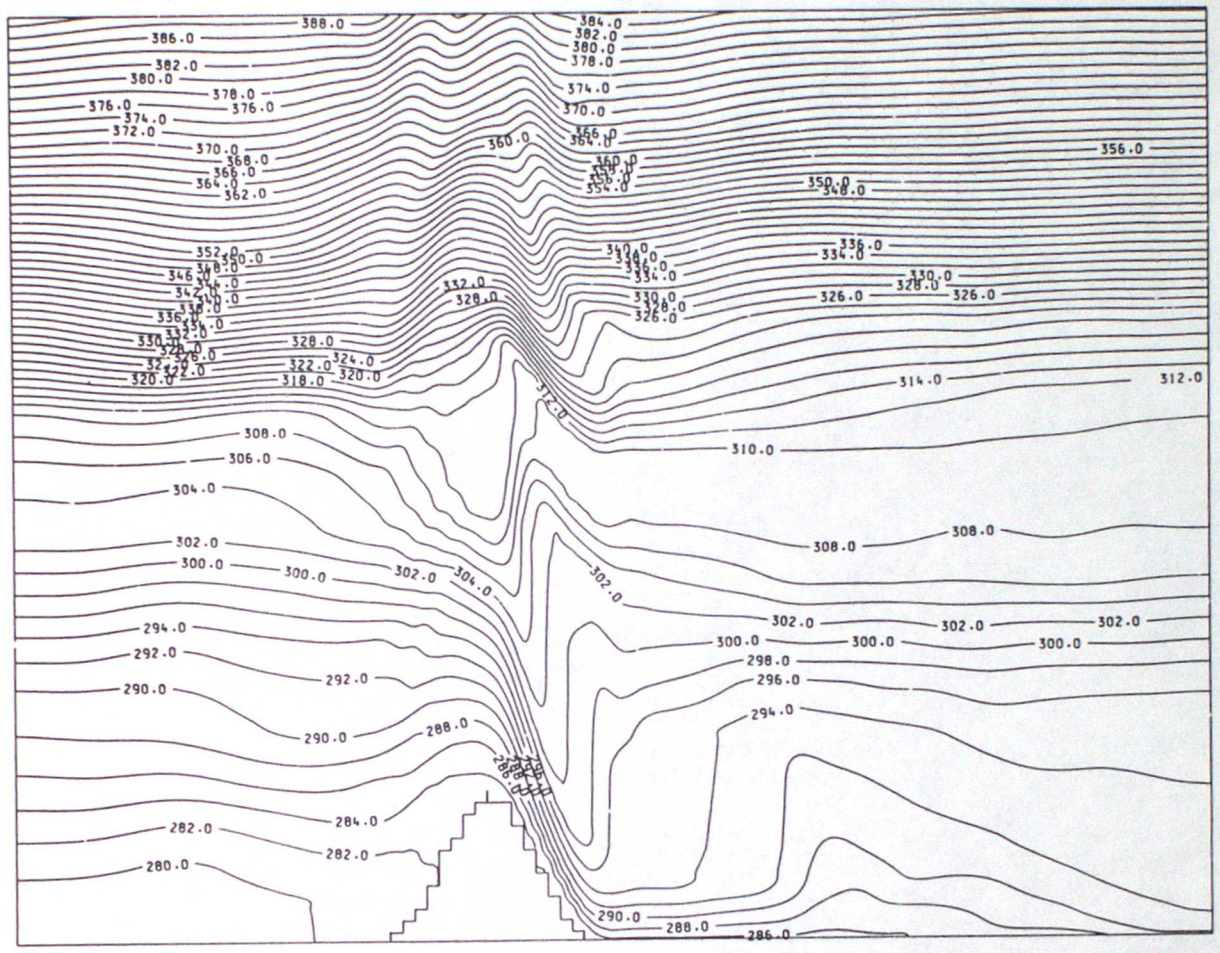
388.0
386.0
384.0
382.0
380.0
378.0
376.0
374.0
372.0
370.0
368.0
366.0
364.0
362.0
360.0
358.0
356.0
354.0
352.0
350.0
348.0
346.0
344.0
342.0
340.0
338.0
336.0
334.0
332.0
330.0
328.0
326.0
324.0
322.0
320.0
318.0
316.0
314.0
312.0
310.0
308.0
306.0
304.0
302.0
300.0
298.0
296.0
294.0
292.0
290.0
288.0
286.0
284.0
282.0
280.0

Fig. 6

Fig. 7

15.0
15.0
15.0
15.0
15.0
20.0
20.0
25.0
30.0
50.0
0.0
10.0
5.0
0.0
5.0
10.0
15.0
20.0
25.0
15.0
10.0
5.0
0.5
15.0
10.0
10.0
15.0
15.0
15.0
15.0
15.0
15.0
15.0
15.0
15.0

Fig. 8 (a)

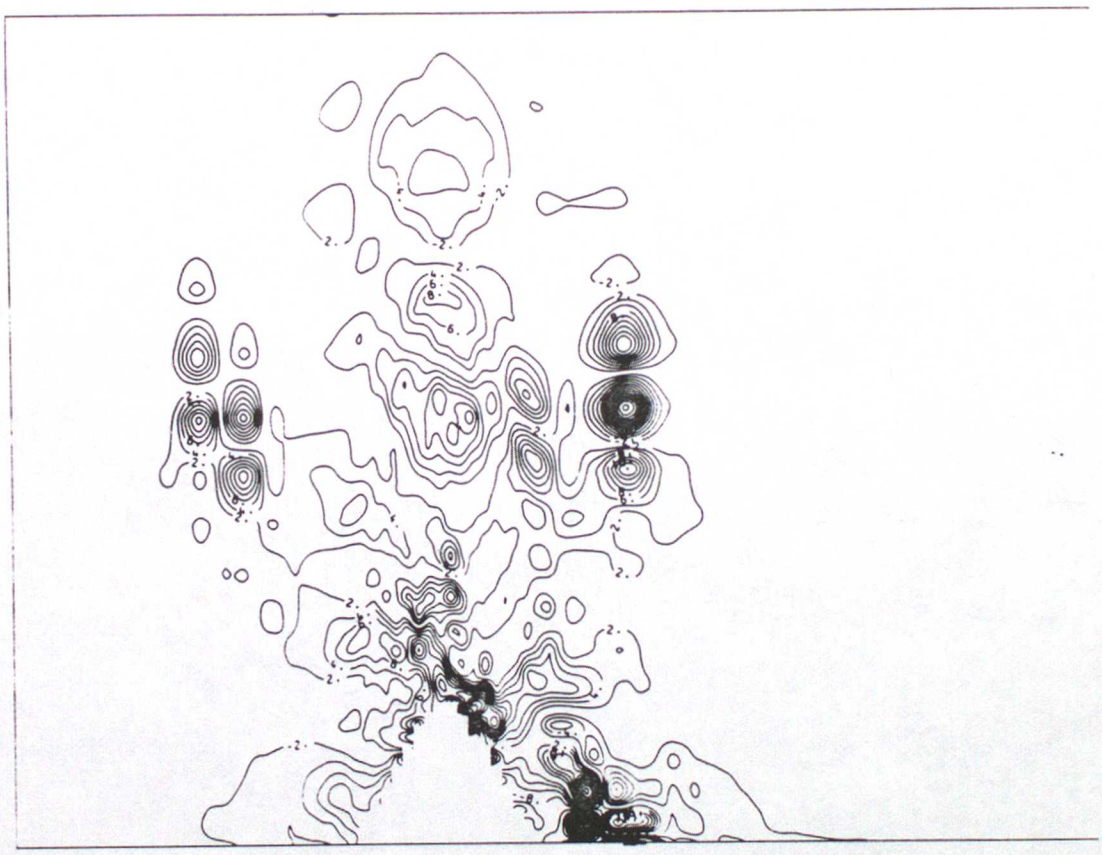

Fig 8 (b)

Fig. 6

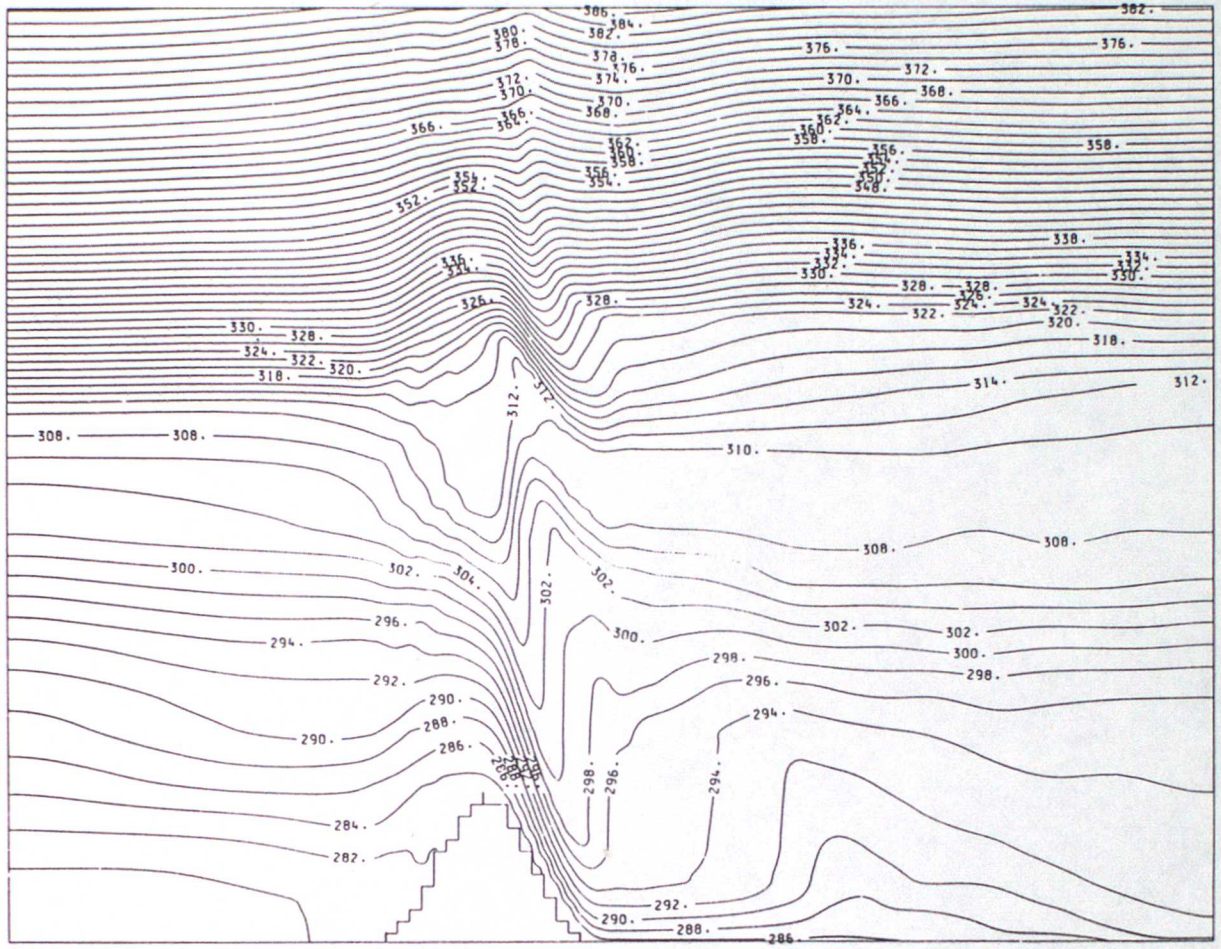
386.
384.
382.
380.
378.
376.
374.
372.
370.
368.
366.
364.
362.
360.
358.
356.
354.
352.
350.
348.
346.
344.
342.
340.
338.
336.
334.
332.
330.
328.
326.
324.
322.
320.
318.
316.
314.
312.
310.
308.
306.
304.
302.
300.
298.
296.
294.
292.
290.
288.
286.
284.
282.

FIG. 10